Arabian Journal of Chemistry (2023) **16**, 105066

King Saud University

Arabian Journal of Chemistry

www.ksu.edu.sa
www.sciencedirect.com

ORIGINAL ARTICLE

Corrosion inhibition properties of spinach extract on Q235 steel in a hydrochloric acid medium

Xinhua Liu *, **Yongguang Gao, Junxia Guan, Qing Zhang, Yu Lin, Chunjie Shi, Ying Wang, Jiarui Du, Nan Ma**

Department of Chemistry, Tangshan Normal University, Tangshan 063000, Hebei, China

Received 1 February 2023; accepted 8 June 2023
Available online 14 June 2023

KEYWORDS

Spinach extract;
Chlorophyll;
CI;
Langmuir monolayer adsorption;
Quantum chemical calculations (QCC)

Abstract The use of environmentally friendly corrosion inhibitors (CIs) is an effective way to overcome the environmental problems caused by existing CIs that contain nitrogen or phosphorus components. Plant extracts, as a type of environmentally friendly CI, have attracted considerable attention. In this work, the corrosion inhibition properties of spinach extract (AESPE) on Q235 steel were studied in a hydrochloric acid medium. First, AESPE was extracted from spinach by an ethanol-acetone reflux method and its main structural and stability parameters in hydrochloric acid medium were determined by infrared spectroscopy (FTIR) and ultraviolet spectroscopy (UV–vis). Second, the corrosion inhibition properties of AESPE on Q235 steel in a 0.5 M hydrochloric acid solution were studied by weight loss (WTL), dynamic potential polarisation (PDP), linear polarisation (LPR), electrochemical impedance spectroscopy (EIS) and quantum chemical calculation methods. The results showed that AESPE could significantly slow the corrosion rate (V_{corr}) of Q235 steel in 0.5 M hydrochloric acid medium, which was via a mixed corrosion inhibition mechanism at the cathode and anode. As the AESPE concentration increased, the cathode and anode currents decreased and the active corrosion sites were blocked; thus, the V_{corr} decreased and the corrosion inhibition efficiency (*E (%)*) increased. Under the conditions of 303 K and 300 mgśL^{-1} AESPE, the *E (%)* of AESPE for Q235 steel was > 90%. As the system temperature increased, the *E%* of AESPE for Q235 steel decreased but the extent of this decrease was small. This work shows that AESPE is an environmentally friendly CI with a good corrosion inhibition effect.

* Corresponding author.
E-mail address: hualiyiwang@163.com (X. Liu).

Peer review under responsibility of King Saud University.

Production and hosting by Elsevier

https://doi.org/10.1016/j.arabjc.2023.105066
1878-5352 © 2023 The Author(s). Published by Elsevier B.V. on behalf of King Saud University.

1. Introduction

Carbon steel is broadly applied in vessels, machinery, architectural skeletons, water supply systems, and the oil and power industries due to its high ductility, thermal conductivity and weldability (Ansari et al. 2020, Nasser et al. 2021, Tan et al. 2021, Xu et al. 2020). In the process of pickling and descaling, carbon steel is prone to corrosion, causing equipment damage and environmental pollution (Alibakhshi et al. 2019, Liu et al. 2018, Olasunkanmi et al. 2020, Saleh et al. 2019). Therefore, CIs are usually used in the acidic solutions involved in the above processes to inhibit corrosion (Ghahremani et al. 2021, Ye et al. 2020). Representative corrosion inhibitors (Cis) incorporate inorganics (e.g., nitrite (Frontini et al. 2019), chromate (Somers et al. 2018), molybdate (Kharitonov et al. 2020), polyphosphate (Koudelka et al. 2019) and organics (Fadhil et al. 2019, Ansari et al. 2020). Inorganic CIs form a thin passivation film or precipitating film on the surface of the sample to slow its corrosion (Dong et al. 2012). Unfortunately, these films are not dense and are therefore unsuitable for inhibiting the prolonged corrosion of metallic materials. For organics, an isolation barrier is formed by the chemical or physical adsorption of active constituents containing organic CIs on the surface of the sample (Cao et al. 2021); however, the application of organic CIs is limited due to their adverse environmental impacts.

With the increasing focus on environmental protection, there has been an increasing focus on environmentally friendly CIs (Hossain et al. 2020, Majd et al. 2020, Mobin et al 2020, Elgyar et al. 2021, Qiang et al. 2020). Among these, plant extract CIs have become a new research focus (Ahanotu et al. 2020, Haque et al. 2020, Chaudhary et al. 2021). As the molecular structures of these extracts are similar to those of traditional organic CIs, plant extracts are considered to be a class of CIs with great potential (Liu et al. 2020, Zhang et al. 2020). According to previous studies, plant extracts derived from papaya leaves (Tan et al. 2021(a)), *Passiflora edulis* Sims peel (Lin et al. 2023), lychee fruit (Hang et al. 2020), castor seeds (Indra Priyatharesini et al. 2019),Ficus tikoua leaves (Wang et al. 2019), *Carissa macrocarpa* (El-Asri et al. 2023), rose fruit (Sanaei et al. 2019), *Rheum ribes* (Işgın) flowers (Fatma et al. 2023), lemon balm (Asadi et al. 2019), magnolia grandiflora leaves (Li et al. 2023) and kiwifruit peel (Dehghani et al. 2019) can effectively inhibit metal corrosion in aggressive media (Salleh et al. 2021). The literature (Ansari et al. 2020.; Agbaffa et al. 2021; Hamilt-Aamachree et al. 2020 etc.) is about research on the corrosion inhibition of steel.

Spinach, also known as Persian grass, is a commonly used vegetable. Spinach extract (AESPE) is a mixture in which natural pigment substances such as chlorophyll (green), carotene (orange-yellow) and lutein (yellow) contain polar groups (pyrrole ring, carbonyl, formyl), unsaturated double bond groups and a hydrophobic long-chain hydrocarbon at the end. These functional groups can inhibit the corrosion of metal, conforming to the basic characteristics of plant CIs. Additionally, the chlorophyll molecule contains two parts: the core is a porphyrin ring; the other part is a long side chain of aliphatic hydrocarbons called phytol. Therefore, the heteroatoms, Π-bond structures and hydrophobic carbon chain structures of chlorophyll molecules give anti-corrosion performance. AESPE as a CI has the advantages of being non-toxic, low-cost and easy to obtain. Therefore, AESPE is an environmentally friendly CI with great development potential. However, to the best of our knowledge, the inhibition action of AESPE on Q235 steel in hydrochloric acid has not been reported.

In this work, AESPE was extracted from spinach by an ethanol-acetone reflux method. The main structural properties and stability of AESPE in an acidic solution were determined by FTIR and UV–vis spectroscopy. Additionally, the ability of AESPE to inhibit the corrosion of Q235 steel in harsh acidic solutions was explored using weight loss (WTL), dynamic potential polarisation (PDP), linear polarisation (LPR) and electrochemical impedance spectroscopy (EIS) techniques. The surface morphology of Q235 steel was characterised by scanning electron microscopy (SEM), spectral analysis (EDS) and the contact angle test (CAT). Additionally, the Langmuir model and theoretical simulation were used to investigate the interactions between AESPE and Q235 steel at the molecular level. Finally, the anticorrosive mechanism was discussed. This work provides important suggestions and ideas for the development of new environmentally friendly CIs.

2. Experimental section

2.1. Extraction of AESPE

The spinach was shaded dried and reduced to powder. spinach powder (50 g) was soaked in a 1000 mL of the mixed solution of anhydrous ethanol and acetone with a volume ratio of 1:1, and refluxed at 323 K for 2 h. The obtained mixed liquid was filtered to take away the residue of AESPE. The resulting liquid was concentrated to 40 mL and dried at 323 K for use. Extraction and anti-corrosion application of AESPE are shown in Fig. 1.

2.2. Corrosion inhibition action test of AESPE by WTL, EIS, LPR and PDP

The concentrations of AESPE were 0 ~ 300 mg·L^{-1}, in the weightlessness and electrochemical tests. The WTH adopted a Q235 steel sample of 72.4 mm × 11.5 mm × 2.0 mm with a superficial area of 20 cm^2.

According to the literature (Zhang et al. 2022),V_{corr} and the corrosion inhibition efficiency (E%) was calculated in the test of WTL. The calculation formulas of V_{corr} and E% are described as formulas (1) and (2).

The corrosion rate:

$$V_{corr} = \frac{\Delta m}{S \times T} \tag{1}$$

Where, Δm is a mean weight lost values of sample, S is a area values of sample, and T is an soak period of sample. the units of V_{corr}, Δm, S and T are $mg \cdot cm^{-2} \cdot h^{-1}$, mg, cm^2 and h, respectively.

The corrosion inhibition efficiency ($E\ (\%)$):

$$E(\%) = \frac{V_0 - V_1}{V_0} \times 100 \tag{2}$$

Where, E is the corrosion inhibition efficiency, V_0 and V_1 are corrosion rate in hydrochloric acid with or without AESPE, respectively.

According to reference (Silva et al. 2021), the electrochemical tests (ET) were proceeded by a Zennium Pro constant potential apparatus. The 2 mm diameter cylindrical Q235 sample was the working electrode (WE) and the rest were sealed with polytetrafluoroethylene. Platinum electrode and Hg/Hg_2SO_4 electrode were separately the counter electrode (CE) and the reference electrode (RE). The WE was polished with a SiC sandpaper (grade 800 ~ 1200). Before every test, WE was soaked in the liquid for 30 min to get E_{ocp}. A curve of PDP was tested under the conditions of 303 K, a voltage range and a sweep rate are ± 100 mV and 0.1 mV·s^{-1}, respectively. AC voltage and a range of frequency in tests of EIS are 10 mV and from 10^5 Hz to 0.01 Hz, respectively. LPR was measured at a linear sweep scope of ± 10 mV with a sweep rate of 0.1 mV·s^{-1}. Data of the polarization and impedance were analyzed by the Zahner Analysis software.

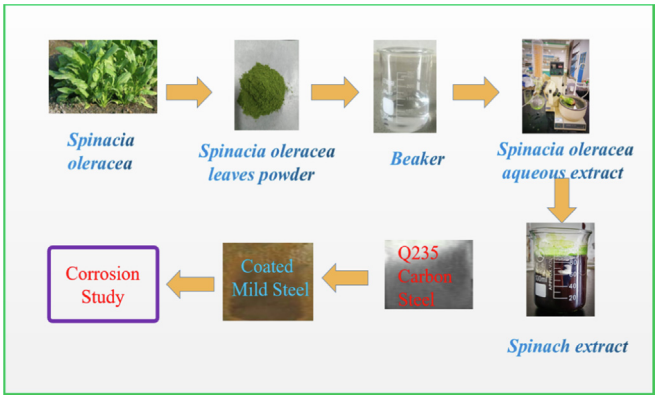

Fig. 1 Illustration of the extraction of AESPE and its anti-corrosion application.

2.3. Structure analysis of AESPE and surface analysis of test samples

The structure of AESPE was analyzed by FTIR (VERTEX7O) and UV–vis (UV-2550). SEM and EDS (A SIGMA 300) were used to analyze the surface appearance and film composition of test sample which were soaked for 8 h. The wettability of the above samples was measured using CAT (JC2000 DM). It was proved that AESPE adsorbed on the surface of the metal samples formed an adsorption film by SEM, EDS and CAT, thus proving that AESPE inhibited the erosion of the metal samples.

2.4. Quantum chemical calculations (QCC)

To get a theoretical Understanding the interaction of the chlorophyll molecule with carbon steel, QCC of the *chlorophyll* molecule were realized in the framework of the density functional theory (DFT) by ORCA 4.0 program package (Neese 2018). The Becke's three-parameter hybrid exchange functional with the Lee-Yang-Parr non-local correlation (B3LYP) (Becke 1993) was employed as the choice for exchange–correlation potential. Grimme's empirical dispersion with Becke-Johnson damping (Grimme et al. 2011) was used to describe the weal intramolecular interactions. The split valence and triple zeta basis sets (def-TZVP) was chosen as basis sets throughou(Schaefer et al. 1994,Schaefer et al. 1992). Optimized geometries were ascertained by vibrational analysis with no imaginary frequency mode.

3. Results and discussion

3.1. Test analysis of AESPE

The FTIR spectra of AESPE and chlorophyll are shown in Fig. 2. The peak at 1065 cm^{-1} corresponds to the pyrrole rings in AESPE. The strong absorption at 1400 cm^{-1} and two moderate absorptions at 1631 and 1739 cm^{-1} confirmed the existence of the C = O and C = C double bond groups in AESPE. The peak at 2927 cm^{-1} corresponded to the stretching and anti-stretching peak of C–H in the aldehyde group of chlorophyll. The wide absorption at 3149 cm^{-1} confirmed the presence of –OH in AESPE. These results revealed that AESPE mainly contained porphyrin ring structures with double bond groups (C = O, C = C and C = N), side-chain aldehyde groups and hydroxyl groups, as in chlorophyll (Wu et al. 2016, Sun 2011). By comparison with the chlorophyll spectrum, it was inferred that the main component of AESPE was chlorophyll.

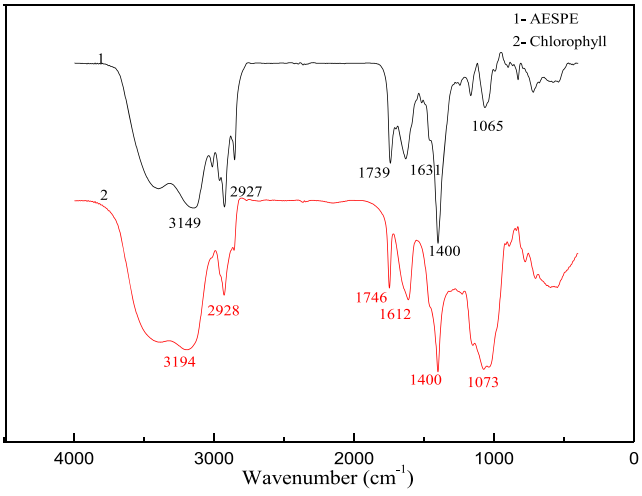

Fig. 2 FTIR spectra of AESPE and chlorophyll.

The UV–vis spectra of chlorophyll and AESPE in hydrochloric acid solution were compared (UV-2550 UV spectrometer, TECHCOMP LIMITED), with the results displayed in Fig. 3. Two peaks appeared at 664/673 nm and 410/416 nm for chlorophyll in [x solution] and in hydrochloric acid (Fig. 3b). The characteristic absorption peak at 664/673 nm indicated that chlorophyll absorbs red light while the characteristic peak at 410/416 nm indicated that chlorophyll absorbs blue-violet light (Wu et al. 2016). As can be seen from Fig. 3a, two characteristic absorption peaks also appeared for the AESPE solution at 414/423 nm and 664/675 nm regardless of the presence of hydrochloric acid medium, further indicating that the main chemical component of AESPE was chlorophyll and, in contrast to the results shown in Fig. 3b, its structure was basically unchanged in hydrochloric acid.

3.2. AESPE corrosion inhibition action test

The corrosion inhibition action test using AESPE was studied by WTL with different concentrations of AESPE and at differ-

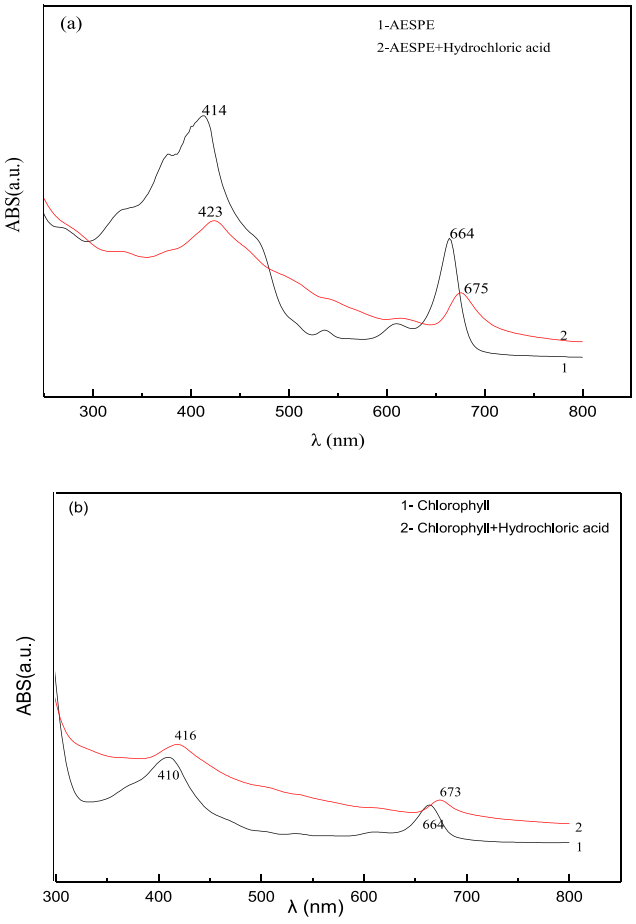

Fig. 3 UV–vis spectra of AESPE and chlorophyll.

ent temperatures. The results are displayed in Table 1. When the amount of AESPE increased from 50 to 300 mg·L^{-1} at 293 ± 3–5 K, E% increased from 48.2% to 95.3%, indicating that V_{corr} decreased and E% increased as the amount of AESPE increased. E% decreased from 95.3% to 88.6% when the test temperature increased from 293 ± 3–5 to 323 ± 3–5 K with 300 mg·L^{-1} of AESPE. This showed that increasing the temperature increased the rate of metal corrosion and led to a decrease in E%, possibly because the dissociation and adsorption equilibrium of AESPE molecules were affected by temperature. The higher the temperature, the more difficult the adsorption of AESPE became, resulting in the formation of a lower-density film and lower E% (Zhang et al. 2017). However, when the temperature was increased to 323 ± 3–5 K, the E% was still as high as 88.6%, indicating that AESPE had good adaptability to temperature changes.

3.3. Corrosion kinetics analysis

The activation energy (E_a), activation entropy (ΔS_a^0) and activation enthalpy (ΔH_a^0) were used to study the kinetics of AESPE. E_a was obtained from the Arrhenius formula (3) (Ituen et al. 2019):

$$\lg V = \frac{-E_a}{2.303RT} + \lg A \quad (3)$$

Table 1 V_{corr} and E% of AESPE.

Temperature (K)	AESPE (mgśL^{-1})	V_{corr} (mgścm^{-2}śh^{-1})	E (%)
293 ± 3–5	0	1.325	–
	50	0.687	48.2
	100	0.302	77.2
	150	0.174	86.8
	200	0.127	90.4
	300	0.062	95.3
303 ± 3–5	0	1.944	–
	50	1.021	47.5
	100	0.467	76.0
	150	0.303	84.4
	200	0.227	88.3
	300	0.109	94.4
313 ± 3–5	0	3.088	–
	50	1.677	45.7
	100	0.855	72.3
	150	0.576	81.3
	200	0.422	86.3
	300	0.253	91.8
323 ± 3–5	0	3.979	–
	50	2.199	44.7
	100	1.245	68.7
	150	0.823	79.3
	200	0.628	84.2
	300	0.452	88.6

Here, V represents the V_{corr} of the Q235 steel sample (Table 1) and T represents the experimental temperature (K).

The relationship between lgV and 1/T is displayed in Fig. S1(a). The values of E_a are shown in Table 2. The change in the slope of the curve indicated that the E_a of the oxidation reaction of the Q235 steel sample changed upon the addition of AESPE. In this experiment, E_a increased from 31.43 to 53.53 kJśmol^{-1} when AESPE was added to the hydrochloric acid solution. This was possibly because the formation of a metal complex upon the adsorption of AESPE blocked the oxidation reaction sites, increasing the E_a required for the metal oxidation reaction.

The transition parameters of the sample dissolution process, ΔS_a^0 and ΔH_a^0, were obtained from the corrosion rate (V) via the weightlessness method (Ituen et al. 2019) using formula (4):

$$\lg \frac{V}{T} = \frac{-\Delta H_a^0}{2.303RT} + \left[\lg \frac{R}{N_A h} + \frac{\Delta S_a^0}{2.303R}\right] \quad (4)$$

Here, N_A is 6.022 × 10^{23} mol^{-1}, h is 6.626 × 10^{-34} Jśs, R is 8.314 JśK^{-1}śmol^{-1} and T (K) is temperature.

Table 2 Sample corrosion parameters.

AESPE (mgśL^{-1})	E_a (kJśmol^{-1})	ΔH_a^0 (kJśmol^{-1})	$-\Delta S_a^0$ (JśK^{-1}śmol^{-1})
0	29.65	27.09	207.43
50	31.43	28.87	206.85
100	38.22	35.66	190.68
150	41.73	39.18	182.98
200	42.71	40.15	182.28
300	53.53	50.97	151.87

The relationship between lg(V/T) and $1/T$ is displayed in Fig. S1(b) and the fitted data are displayed in Table 2. The values of ΔH0a increased with the addition of AESPE. When AESPE reached 300 mg·L^{-1}, the value of ΔH_a^0 increased from 27.09 to 50.97 kJ·mol^{-1}. At each AESPE concentration, ΔH_a^0 was positive, indicating that all corrosion reactions were endothermal. With the addition of AESPE, the rate of the steel corrosion reaction decreased because it required more energy.

Ideally, E_a and ΔH_a^0 should be equal. When E_a is greater than ΔH_a^0, gases are released in the corrosion process; that is, hydrogen is evolved. The parameters in Table 2 show that the difference between the two values ($E_a - \Delta H_a^0$) was nearly constant in all cases, with its average value equal to the value of RT (2.56 kJ·mol^{-1}). Therefore, the number of molecules (χ) in the equation $E_a - \Delta H_a^0 = \chi RT$ was 1 (Silva et al. 2012), which proved that the rate-determining step (RDS) was a single-molecule reaction. The negative value of ΔS_a^0 showed that the activation complex in the RDS formed through association rather than dissociation. The decrease in ΔS_a^0 was caused by the adsorption action of substances that migrated from the solution to the sample surface by electrostatic forces. As a result, the number of freely moving particles in the solution decreased.

When the concentration of AESPE was 300 mg·L^{-1}, ΔS_a^0 increased from –207.43 to –151.87 J·K^{-1} ·mol^{-1}. A few polar molecules and ions on the surface of the sample exchanged with AESPE molecules, releasing the previously adsorbed particles into the solution. The addition of AESPE led to the desorption of H_2O, H_3O^+ and other particles from the sample surface or they could not be adsorbed to the sample surface, which promoted the increased ΔS_a^0 of the system. The adsorbed AESPE molecules played a role in spatial resistance at the interface between the sample and the solution, which reduced the capacity of other particles (mainly H_3O^+) to adsorb and re-adsorb, leading to a decrease in the cathodic reaction rate and thus a slower corrosion rate (Hamilton-Aamachree et al. 2020).

3.4. Adsorption model

The mechanism of interaction between the CI and the sample surface was analysed by adsorption isotherms. The chemical components of the CI, the electrolyte, the metal surface properties and the medium temperature, etc., can affect the adsorption isotherm. Therefore, various isotherms such as Bockris-Swinkels, Langmuir, Freundlich and Temkin etc. were used (Mohammad et al. 2021).

The adsorption action of CI molecules can be classified as physical or chemical adsorption. The former arises from the electrostatic interaction between a charged molecule of CI and the charged sample surface. The latter is a process in which CI heteroatoms provide lone-pair electrons to form a coordinate bond (CB) with the empty orbitals of the metal atoms (EOMA). The adsorption process in the current study can be described by the following process (Tan et al. 2021(b)):

$$AESPE_{(sol)} + \chi H_2O_{(ads)} \Longleftrightarrow AESPE_{(ads)} + \chi H_2O_{(sol)}$$

Here, $H_2O_{(ads)}$ is an adsorbed water molecule and $AESPE_{(ads)}$ is an adsorbed molecule of AESPE. Thus, the formation of an adsorption thin film at the sample/solution interface is a process of substituting water molecules.

To further study the interaction mechanism of AESPE at the sample/solution interface, Langmuir and Temkin isotherms were fitted with the data from the weightlessness test data. The results are displayed in Fig. S2, S3 and S4.

1) Langmuir isotherm

$$\frac{c}{\theta} = \frac{1}{K_{ads}} + c \tag{5}$$

Here, K_{ads} is the equilibrium constant.

The relationship between C/θ and C is shown in equation (5). Fig. S2 shows the adsorption isotherm of AESPE. K_{ads} was obtained from the intercept of the line. The standard adsorption free energy (ΔG_{ads}^0) is shown in equation (6) (Mohammad et al. 2021):

$$\Delta G_{ads}^0 = -RT\ln(C_{H_2O}K_{ads}) \tag{6}$$

Here, the pure water concentration (C_{H2O}) is 10^3 g·L^{-1}. The mean value of ΔG_{ads}^0 was –25.16 kJ·mol^{-1} (Table 3). According to the literature (–40 kJ·mol^{-1} < ΔG_{ads}^0 < –20 kJ·mol^{-1}, (Wang et al. 2019), this indicated that the adsorption of AESPE was due to the coexistence of physical and chemical adsorption and that this adsorption was spontaneous. When the AESPE molecule approached the surface of the sample, the electrostatic attraction was unquestioned; this can be viewed as physical adsorption. The coordination behaviour of the lone-pair electrons of the AESPE molecules and EOMA suggested the presence of chemisorption.

The standard adsorption enthalpy and entropy (ΔH_{ads}^0 and ΔS_{ads}^0) can be calculated from equation (7) (Mohammad et al. 2021).

$$\ln K = -\frac{\Delta H_{ads}^0}{RT} + \frac{\Delta S_{ads}^0}{R} - \ln C_{H_2O} \tag{7}$$

Here, ΔH_{ads}^0 andΔS_{ads}^0 come from the slope and intercept of the line in Fig. S3, with values of –3.91 and 69.12 J·K^{-1}·mol^{-1}, respectively. ΔH_{ads}^0 was negative, indicating that the adsorption of AESPE was exothermic. $\Delta S_{ads}^0 > 0$ indicated that the adsorption of AESPE was an entropy-increasing action. Generally, the adsorption action of a CI on a sample surface is an entropy-decreasing process but, in this experiment, the adsorption of the CI was a process of increasing entropy. This was possibly due to the desorption of water molecules and the adsorption of AESPE, with multiple water molecules desorbing for every one molecule of AESPE that adsorbed on the Q235 surface. This substitution of multiple H_2O or H_3O^+ molecules by one AESPE molecule increased the degree of chaos; that is, the entropy of the whole system increased, with $\Delta S_{ads}^0 > 0$ (Wang et al. 2019, Ateya et al. 1984).

Table 3 Thermodynamic parameters obtained from the adsorption of AESPE on Q235.

$T\ (K)$	$K_{ads}(L \cdot g^{-1})$	R^2	$\Delta G_{ads}^0(kJ \cdot mol^{-1})$
293 ± 3–5	19.96	0.9914	−24.12
303 ± 3–5	19.19	0.9932	−24.84
313 ± 3–5	17.83	0.9942	−25.47
323 ± 3–5	17.36	0.9947	−26.22

2) Temkin isotherm

The Temkin isotherm can be described by equations (8) and (9):

$$\exp(-2a[03B8]) = KC \tag{8}$$

$$\theta = -\frac{2.303\log K}{2a} - \frac{2.303\log C}{2a} \tag{9}$$

Here, a is the molecular interaction parameter. The relationship between θ and log C is displayed in Fig. S4. The parameters in Table 4 were calculated according to the Temkin isotherm in Fig. S4. At different temperatures, all values of a were negative, indicating a repulsive force between the adsorbed molecules. The R^2 value from the fitted Temkin adsorption curve showed that there was a modest correlation between θ and log C for the corrosion inhibition system. Therefore, The Langmuir adsorption isotherm provided a better fit for the test data than the Temkin isotherm. Thus, the Langmuir isotherm was more suitable for describing the corrosion inhibition action of AESPE, which confirmed that AESPE participated in a single-layer adsorption process in the hydrochloric acid system (Tan et al. 2021(a)).

3.5. Polarisation test

The instantaneous corrosion rate and the electrochemical reaction mechanism were studied using the polarisation method. The E_{OCP}, PDP and LPR curves for the Q235 sample are displayed in Fig. 4 and Fig. 5.

1. E_{OCP} tests

Fig. 4 shows the E_{OCP} curves. The curve stabilised after the Q235 sample had been immersed in the acid solution for 30 min, indicating that the sample surface reached a stable state. Additionally, E_{OCP} stabilised at − 957 mV in hydrochloric acid without AESPE, as a consequence of the dissolution of the Q235 sample in the acid. With the addition of AESPE, the E_{OCP} curves tended to move towards the anode, indicating that the adsorption of AESPE inhibited the active sites of the anodic reaction, thus showing excellent corrosion inhibition effect (Chen et al. 2020).

2. LPR tests

The polarisation resistance (Rp) values derived from the LPR tests are displayed in Table 5. The *E (%)* value can be calculated using equation (10):

$$E(\%) = (1 - \frac{R_p^0}{R_p}) \times 100 \tag{10}$$

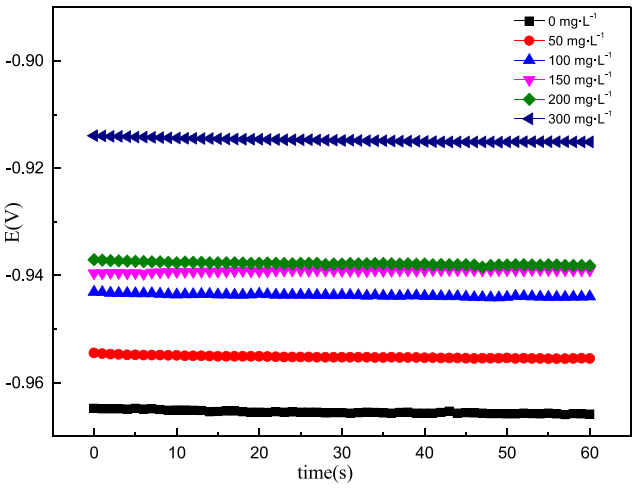

Fig. 4 E_{ocp}-t curves of Q235 steel with and without AESPE in 0.5 M hydrochloric acid.

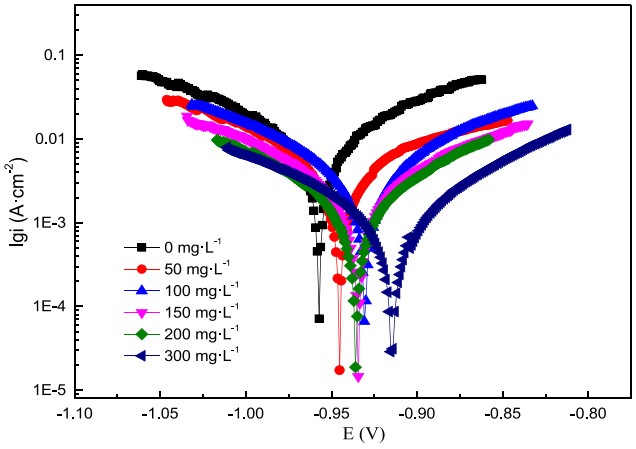

Fig. 5 Polarisation curves of the Q235 sample in hydrochloric acid with or without AESPE.

Here, R_p^0 and R_p are the polarisation resistance in hydrochloric acid without AESPE or with AESPE, respectively.

The R_p gradually increased as the AESPE concentration increased (Table 5). The R_p decreased from 26.09 Ω·cm^2 in 0.5 M hydrochloric acid containing 300 mg·L^{-1} AESPE to 2.52 Ω·cm^2 at 0.5 M hydrochloric acid (blank). The R_p increased in the system with AESPE, indicating that a non-conductive adsorption film was formed in the interface

Table 4 Thermodynamic parameters derived from the Temkin isotherm in hydrochloric acid.

Temperature (K)	Intercept	Slope	R^2	–a	K	ΔG^0_{ads} (kJ·mol^{-1})
293 ± 3–5	1.3233	0.6066	0.9245	1.90	151.77	−29.06
303 ± 3–5	1.3001	0.5969	0.9355	1.93	150.64	−30.03
313 ± 3–5	1.2711	0.5936	0.9493	1.94	138.52	−30.81
323 ± 3–5	1.2311	0.5750	0.9542	2.00	137.48	−31.77

between the Q235 sample and the solution (Mourya et al. 2014).

3. PDP tests

Fig. 5 shows the polarisation action of the Q235 sample. The *E (%)* value of AESPE was derived using equation (11) and the results are shown in Table 5.

$$E(\%) = \frac{i^0_{coor} - i_{coor}}{i^0_{coor}} \times 100 \quad (11)$$

Here, i_{corr} and i^0_{corr} are the current densities in 0.5 M hydrochloric acid with AESPE and without AESPE, respectively.

As the concentration of AESPE increased, the anodic and cathodic curves shifted towards lower i_{corr} values, resulting in a decrease in i_{corr}. AESPE significantly inhibited both the cathodic and anodic reactions of the Q235 sample electrode. The corrosion potential (E_{corr}) shifted towards a higher potential with the addition of AESPE, indicating that more AESPE molecules were adsorbed on the anode, thus preventing the anodic reaction. In general, an absolute displacement of E_{corr} of less than 85 mV compared to the E_{corr} in the blank solution is indicative of a mixed corrosion inhibition mechanism(Tan et al. 2021 (b)).In this work, the maximum displacement was 42 mV, indicating that AESPE was a mixed-type CI. The Tafel slopes of β_a and β_c showed similar changes in the AESPE system, indicating that the reaction mechanism of the sample did not change. The inhibition mode of organic CIs can be classified into three types: the geometric covering effect (GCE) of adsorbed CIs, the blocking effect of active sites (BEAC) of adsorbed CIs, and the electrocatalytic effect (EE) of CIs (Cao. 1996). In the GCE, the protective effect derives from a reduction in the reaction area of the corroded sample. In the other two modes (BEAC and EE), the inhibition effect derives from the change in E_a of the anodic and cathode reactions during the corrosion reaction. According to the polarisation reaction results, the addition of AESPE resulted in changes in the βa and βc, indicating that the inhibition was probably caused by two modes (GCE and BEAC). The similar cathodic Tafel line in Fig. 5 showed that AESPE did not change the hydrogen evolution reaction mechanism and the reduction of H^+ ions; but mainly occurred through the charge transfer mechanism (Chen et al. 2020).

3.6. EIS test

EIS test results can provide information on the sample/electrolyte interface reaction. In this work, EIS tests were conducted on Q235 samples in 0.5 M hydrochloric acid with or without AESPE. The results are shown in Fig. 6 and Fig. 7. The Nyquist diagram contained an irregular semicircle for each condition in Fig. 6, which may have been due to the non-uniform surface of the Q235 sample. The semicircle diameter increased significantly as the AESPE increased, indicating that AESPE improved the E%, which may have been related to the adsorption of the chlorophyll from AESPE on the Q235 sample. As shown in the Bode diagram (Fig. 7), an increase in the concentration of AESPE increased the Bode modulus impedance and phase angle, indicating a delay in the corrosion reaction process.

An equivalent circuit in Fig. S4 was fitted by the EIS data and the parameters are displayed in Table 6. Therein, R_s and R_{ct} are the solution resistance (SR) and the charge transfer resistance (CTR), respectively. CPE reflects the replacement of the double-layer capacitor by the constant phase element. The χ^2 values in Table 6 ranged from 0.00259 to 0.00927, indicating that the circuit in Fig. S4 agreed with the EIS data.

The value of E% could be calculated using equation (12):

$$E(\%) = \frac{R_{ct} - R_{ct0}}{R_{ct}} \times 100 \quad (12)$$

Here, R_{ct} and R^0_{ct} are the CTR in the presence and absence of AESPE, respectively.

Z_{CPE} is defined by equation (13):

$$Z_{CPE} = Y_0^{-1}(j\omega)^{-n} \quad (13)$$

Here, Y_0 is the CPE constant, j is the imaginary root, n is the offset—which is defined as the deviation from the ideal value, usually between 0 and 1, and w is the angular frequency.

The interface dual capacitance (C_{CPE}) value was obtained from equation (14):

$$C_{CPE} = \frac{1}{2\pi f_{max}(-Z''_{(max)})R_{ct}} \quad (14)$$

Here, $f_{max}(-Z''_{(max)})$ is the maximum value of the imaginary component of impedance.

The R_{ct} value in the system containing AESPE was much larger than the R_{ct0} value in the system without AESPE. The effectiveness of AESPE could be ascribed to the adsorption of chlorophyll molecules. Chlorophyll would coexist as both the molecular and protonated form in the acidic medium. The relative concentrations of these two forms would depend on the degree of protonation. It is possible that coordination bonds formed between the lone-pair electrons or conjugated double bonds of the O and N atoms of the chlorophyll molecule (or its protonated form) and EOMA in the Q235 sample. Thus, adsorption occurred, which plays a better corrosion

Table 5 Dynamic potential polarisation and linear polarisation of Q235 sample in hydrochloric acid with or without AESPE.

c_{inh} ($g{\cdot}L^{-1}$)	β_a($mV{\cdot}dec^{-1}$)	β_c($mV{\cdot}dec^{-1}$)	I_{corr} ($mA{\cdot}cm^{-2}$)	E_{corr} (mV)	E_{PDP} (%)	R_p ($\Omega{\cdot}cm^2$)	E_{LPR} (%)
0	194	200	19.71	−57	–	2.52	–
50	147	168	10.67	−938	45.88	4.49	43.64
100	133	145	5.67	−930	71.24	11.81	78.64
150	157	138	3.79	−934	80.77	16.30	84.53
200	126	129	2.57	−936	86.98	20.91	87.94
300	104	124	1.41	−915	92.83	26.09	90.33

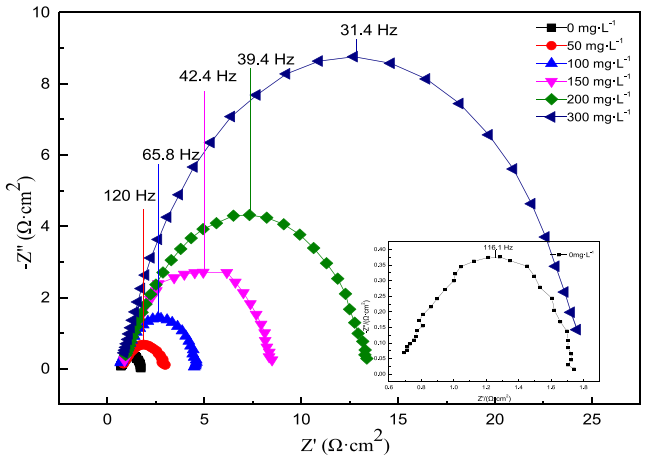

Fig. 6 Nyquist diagrams of the Q235 sample in hydrochloric acid with or without AESPE.

inhibition performance. This was in accordance with the *E (%)* values calculated by the weightlessness method and the two different electrochemical calculations, above.

3.7. Surface analysis

Surface analysis technologies were used to describe the surface state of the Q235 sample and prove the adsorption of AESPE. In this work, the SEM, EDS and CAT surface analysis methods were used. Fig. 8(a, c, e) shows the appearance of the Q235 sample surface before corrosion, in hydrochloric acid and in hydrochloric acid with 300 mg·L^{-1} AESPE. Under 1000x magnification, the surface of the Q235 sample before corrosion had mechanical grinding scratches and was smooth. The surface of the sample soaked in hydrochloric acid was seriously corroded. After the addition of AESPE, there was almost no accumulation of corrosion; rather, the sample was covered with a protective layer. The chlorophyll molecules in AESPE adsorbed on the Q235 sample, preventing the diffusion of corrosive ions such as Cl^-, thereby decreasing the extent of the corrosion reaction. This proved that AESPE had a good protective effect on the metal Q235 sample in hydrochloric acid.

To provide insight into the adsorption of AESPE on the surface of the Q235 sample, EDS analysis was performed on new uncorroded samples and samples in hydrochloric acid with or without AESPE. The results are displayed in Fig. 8b, d and f. Fig. 8d shows that the oxygen content of the sample in hydrochloric acid solution increased compared with that prior to corrosion (Fig. 8b). The hydrochloric acid solution promoted the oxidation reaction, generating more iron oxides from corrosion and resulting in increased oxygen content. Significantly, corrosive Cl^- ions appeared in the EDS spectra of the Q235 sample surface in hydrochloric acid. However, when AESPE was present in the test solution (Fig. 8f), the characteristic O peak was considerably reduced, indicating that very few oxides were produced on the sample surface due to corrosion. In fact, the oxygen content was almost the same as that before corrosion.

These test results showed that the adsorption of molecules of AESPE on the surface of the sample prevented the diffusion of Cl^- and reduces the formation of corrosion products

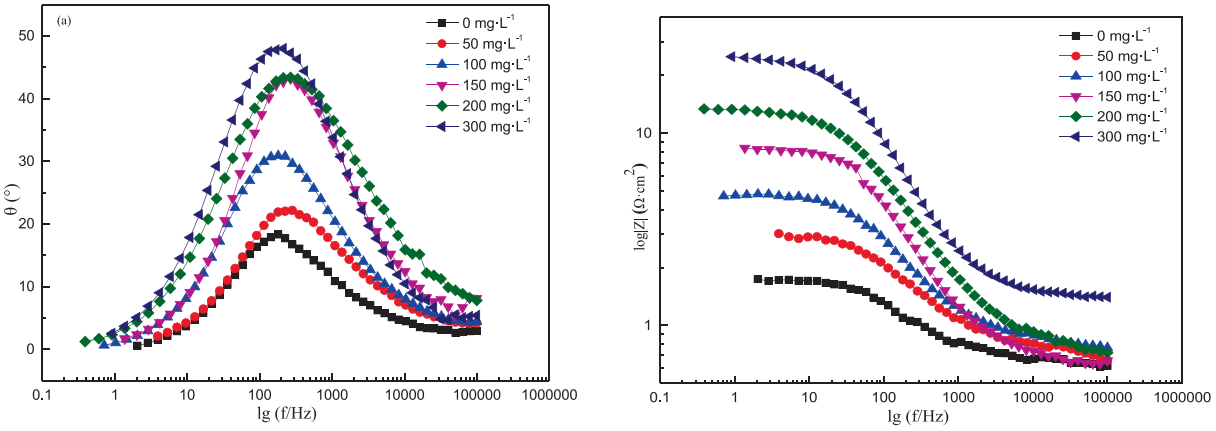

Fig. 7 Bode diagrams of the Q235 sample in hydrochloric acid with or without AESPE.

Table 6 Results of EIS tests in hydrochloric acid with or without AESPE.

C_{inh} (mg·L^{-1})	R_s (W·cm^{-2})	Y_0 (S·W·cm^{-2})	R_{ct} (W·cm^{-2})	n	C_{CPE} (mF·cm^{-2})	χ^2	E (%)
0	0.65	8469.74	1.13	0.705	1212.87	0.00268	–
50	0.73	5185.99	2.23	0.673	590.99	0.00496	49.22
100	0.81	3238.53	4.21	0.714	583.22	0.00401	73.13
150	0.66	1284.94	7.66	0.773	490.28	0.00927	85.24
200	0.72	1562.13	13.41	0.701	301.40	0.00530	91.57
300	1.41	657.01	24.30	0.783	208.59	0.00259	95.35

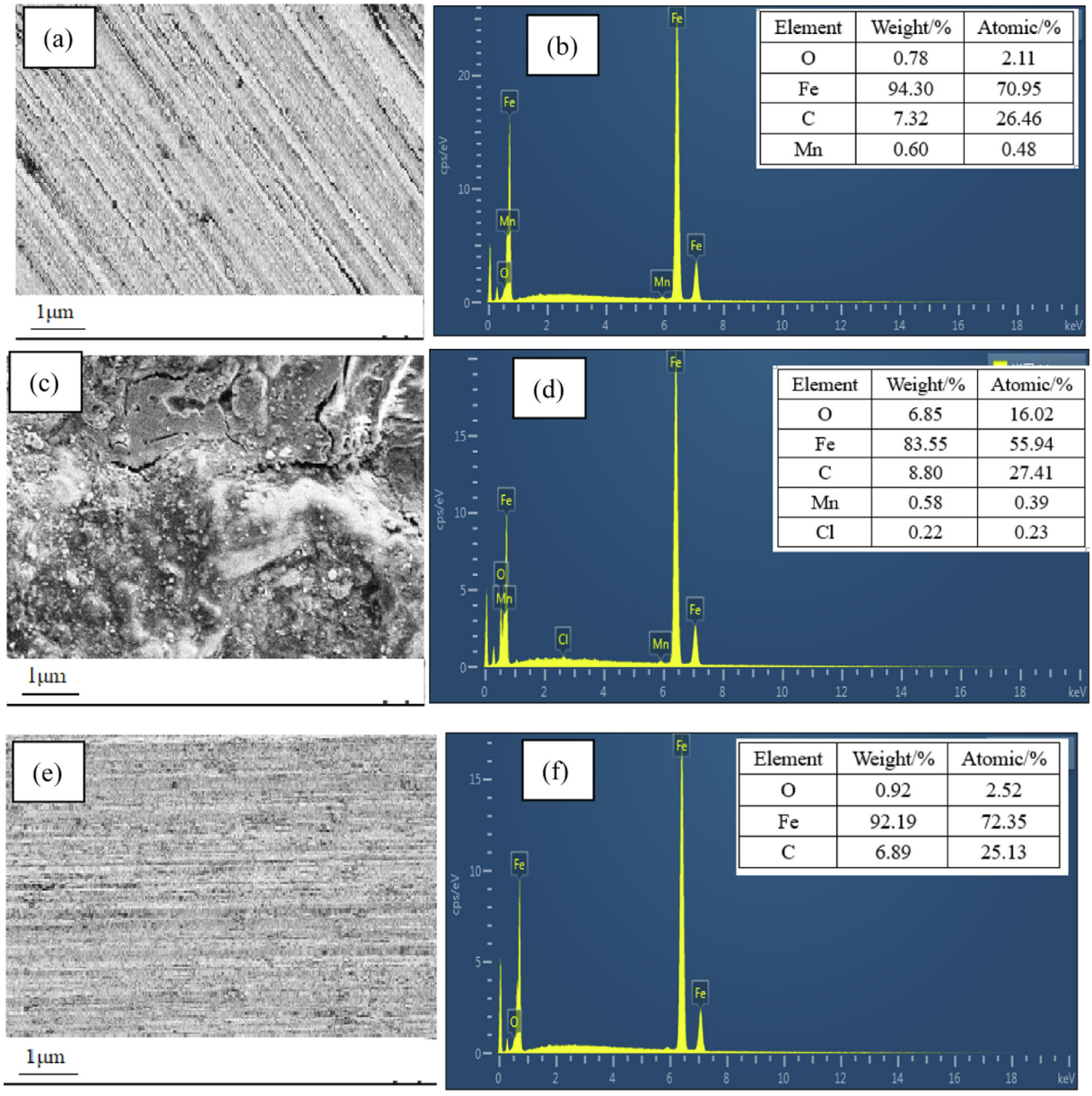

Fig. 8 SEM images and EDS spectra of Q235 steel surface. (a, b) New uncorroded sample, (c, d) sample in hydrochloric acid, (e,f) sample in hydrochloric acid with AESPE.

(Fe_2O_3, $FeCl_3$ and other complexes). Consequently, the surface of the Q235 sample was highly resistant to the diffusion of strong acid ions, increasing the values of E%. These test results were in accordance with the results obtained by SEM.

The contact angle, which is the angle formed between a sample surface and a liquid–vapour interface, can be used to characterise the wettability of a sample surface. In this work, the hydrophobicity of the sample surface before and after corrosion was ascertained through the contact angle, and thus the adsorption characteristics of AESPE on the Q235 sample surface were verified. As displayed in Fig. S6a, for newly polished Q235 steel, the observed contact angle was very large (102°), indicating that the sample had good hydrophobicity. As shown in Fig. S6b, after the sample was immersed in hydrochloric acid at 303 K for 8 h, the contact angle of the Q235 sample surface was 65°, indicating that the hydrophobicity had decreased. Fig. S6c shows that the contact angle of the sample with 300 mgɬL^{-1} AESPE was 94°, indicating that the surface hydrophobicity was somewhat reduced compared with the newly polished surface, but much greater than that in hydrochloric acid. This was due to the adsorption of AESPE molecules on the Q235 sample to form a hydrophobic layer (Mohammad et al., 2021). Therefore, the presence of AESPE could decrease the value of V_{corr} of Q235 steel and improve the value of E%.

3.8. Quantum chemical calculations

The electronic properties of an organic compound are important in predicting its reactivity on a sample surface. According

to molecular orbital theory, the frontier orbital energy levels (E_{HOMO} and E_{LUMO}) are closely related to the reaction of a CI (Umoren et al. 2015, Zhang et al. 2018). Therefore, the E_{HOMO} and E_{LUMO} of a chlorophyll molecule are of great significance to the discussion of its interaction with the steel surface. As shown in Fig. S7, the HOMO and LUMO of a chlorophyll molecule are located in the porphyrin ring. This distribution of the molecular orbitals of a chlorophyll molecule provided more active sites for AESPE, enabling it to obtain more free electrons from the iron via the antibonding orbitals and to supply more electrons to the EOMA. E_{HOMO} and E_{LUMO} represent the ability of a molecule to supply electrons and to receive electrons, respectively (Hu et al. 2017). That is, a higher E_{HOMO} or a lower E_{LUMO} indicates that a CI molecule is more likely to share electrons with a metal sample, so the E % is higher (Zhang et al. 2018). On the other hand, the smaller the ΔE ($\Delta E = E_{LUMO} - E_{HOMO}$), the higher the reactivity of the system and the higher E% is (Umoren et al. 2015). The electron transfer percentage (ΔN) is the amount of electron transfer from the CI to the sample. When ΔN is less than 3.6, the larger the ΔN value, the higher E% is (Ghailane et al. 2017). ΔN can be calculated based on η and χ, as shown in equations (15)–(17) (Zhang et al. 2018, Yilmaz et al. 2016).

$$\Delta N = \frac{\chi_{Fe} - \chi_{inh}}{2(\eta_{Fe} + \eta_{inh})} \tag{15}$$

$$\eta = \frac{E_{LUMO} - E_{HOMO}}{2} \tag{16}$$

$$\chi = \frac{-E_{HOMO} - E_{LUMO}}{2} \tag{17}$$

Here, η_{inh} and χ_{inh} represent the hardness and electronegativity of the CI, respectively. For iron, χ_{Fe} is 7 eV$\cdot$mol^{-1} and η_{Fe} is 0 eV$\cdot$mol^{-1} (Obi-Egbedi et al. 2011, Yadav et al. 2010). The data are presented in Table 7. Not only did chlorophyll have high E_{HOMO} and ΔN values, but it also had low E_{LUMO} and ΔE values, which theoretically explained the corrosion inhibition ability of AESPE in hydrochloric acid. These QCC results further validated the experimental results.

3.9. Corrosion inhibition mechanism

In an acidic medium, the corrosion inhibition process usually derives from the adsorption of the CI on the sample. The experimental results showed that AESPE underwent both chemical adsorption and physical adsorption on the steel sample in hydrochloric acid, which made it a mixed-type CI. During the interaction between the Q235 steel and AESPE, on the one hand, negatively charged ions (such as Cl^-) in the acidic medium attracted positively charged AESPE ions through electrostatic attraction (physical adsorption). In the acidic solution, AESPE existed primarily as protonated ions, which attached directly to the cathode on the surface of the Q235 sample, thereby reducing the hydrogen evolution process. On the other hand, the anodic dissolution of the sample was reduced by chemisorption at the anode. Thus, the inhibitory mechanism of AESPE resulted from physical adsorption and chemical adsorption processes of the main component of AESPE(chlorophyll) on the sample surface.

3.10. Comparison of the corrosion inhibition action of AESPE with other CIs

A variety of CIs—including alanine and leucine (amino acids), TMA and TML (ionic liquids), and *Mimosa pudica*, LB.E, BLE (plant extracts) have been developed. Their corrosion inhibition properties are shown in Table 8. As a comparison, the corrosion inhibition properties of AESPE determined in the present study are also listed in Table 8. The E% of steel generally ranged from 56.6% to 94.50% under the experimental conditions of 298 to 303 K in hydrochloric acid solution. AESPE had a good anti-corrosion effect, with a maximum cor-

Table 7 QCC parameters for chlorophyll.

CI	E_{HOMO} (eV)	E_{LUMO} (eV)	ΔE (eV)	ΔN (eV)	χ (eV)	η (eV)
Chlorophyll	−5.212	−2.841	2.371	1.253	4.027	1.186

Table 8 Comparison of the properties of different CIs in hydrochloric acid.

CI	Sample	Temperature (K)	C_{inh}	η (%)	Ref.
Alanine	Mild steel	298	10^{-3} M	79.0	(Khaled et al. 2012)
		303	0.5 g/L	56.6	(Eddy et al. 2011)
Leucine	Mild steel	303	0.5 g/L	64.4	(Eddy et al. 2011)
		298	0.1 M	91.6	(Ashassi-Sorkhabi et al. 2004)
TMA	X52 steel	298	0.1 g/L	70.0	(Xomet et al. 2014)
TML		298	0.1 g/L	70.0	(Xomet et al. 2014)
[PheME][Sac]	Mild steel	303	0.1 g/L	79.5	(Aslam et al. 2020)
Mimosa pudica	Mild steel	298	1.0 g/L	77.3	(Agbaffa et al. 2021)
LB.E	Mild steel	298	0.8 g/L	94.5	(Asadi et al. 2019)
BLE	Q235 steel	298	0.4 g/L	93.8	(Tan et al. 2021(a))
AESPE	Q235 steel	303	0.3 g/L	93.2	(This work)

rosion inhibition efficiency (η_{Max}) of 93.2% at 0.3 $g\dot{s}L^{-1}$ AESPE. The corrosion inhibition performance of AESPE was basically the same as that of other plant extracts but better than that of amino acids and ionic liquids. Additionally, as shown in Table 8: (i) AESPE was a good CI, considering the concentration of CI required and its corrosion inhibition efficiency; and (ii) plant-extracted CIs are increasingly favoured by researchers, based on the development history of environmentally friendly CIs. Therefore, AESPE is a good CI with bright application prospects.

4. Conclusion

The main component of AESPE is chlorophyll and it is stable in 0.5 M hydrochloric acid medium. AESPE could significantly decrease the V_{corr} of a Q235 sample in hydrochloric acid as a mixed-type CI, inhibiting the cathode and anode. As the concentration of AESPE increased, the current density decreased and the active corrosion sites were blocked, resulting in a decrease in V_{corr} and an increase in E%. The E% value was above 90% at 303 K when the AESPE concentration was 300 $mg{\cdot}L^{-1}$. The adsorption of AESPE on the Q235 sample surface conforms to the Langmuir isothermal equation, indicative of monolayer adsorption. QCC showed that the corrosion inhibition performance of AESPE was mainly due to the charge transfer between AESPE and the metal, facilitating the absorption of AESPE molecules on the sample surface. The QCC results were basically in accordance with the experimental results. In conclusion, AESPE is an environmentally friendly CI for steel.

Declaration of Competing Interest

The authors declare that they have no known competing financial interests or personal relationships that could have appeared to influence the work reported in this paper.

Acknowledgements

This work was financially supported by the Natural Science Foundation of Hebei Province of China (D2022105004), the Foundation of Tangshan Normal University of China (2022C42) and the Foundation of Phased Achievement of the Key Cultivation Project of Tangshan Normal University of China (ZDPY07, ZDPY05).

Appendix A. Supplementary material

Supplementary data to this article can be found online at https://doi.org/10.1016/j.arabjc.2023.105066.

References

Agbaffa E.B., Akintemi E.O., Uduak E.A., et al. 2021. Corrosion inhibition potential of the methanolic crude extract of Mimosa pudica leaves for mild steel in 1 M hydrochloric acid solution by weight loss method. Science Letters, 15:23-42. https://doi.10.24191/sl.v15i1.11791Corpus ID: 234317168.

Ahanotu, C.C., Onyeachu, I.B., Solomon, M.M., et al, 2020. Pterocarpus santalinoides leaves extract as a sustainable and potent inhibitor for low carbon steel in a simulated pickling medium. Sustain. Chem. Pharm. 15,. https://doi.org/10.1016/j.scp.2019.100196 100196.

Alibakhshi, E., Ramezanzadeh, M., Haddadi, S.A., et al, 2019. Persian Liquorice extract as a highly efficient sustainable CI for mild steel in sodium chloride solution. J. Clean. Prod. 210, 660–672. https://doi.org/10.1016/j.jclepro.2018.11.053.

Ansari, K.R., Chauhan, D.S., Quraishi, M.A., et al, 2020. Bis(2-aminoethyl)amine-modified graphene oxide nanoemulsion for carbon steel protection in 15% HCl: effect of temperature and synergism with iodide ions. J. Colloid Interface Sci. 564, 124–133. https://doi.org/10.1016/j.jcis.2019.12.125.

Asadi, N., Ramezanzadeh, M., Bahlakeh, G., et al, 2019. Utilizing Lemon Balm extract as an effective green CI for mild steel in 1M HCl solution: a detailed experimental, molecular dynamics, Monte Carlo and quantum mechanics study. J. Taiwan Inst. Chem. Eng. 95, 252–272. https://doi.org/10.1016/j.jtice.2018.07.011.

Ashassi-Sorkhabi H., Majidi M.R., Seyyedi K., 2004. Investigation of inhibition effect of some amino acids against steel corrosion in HCl solution. Appl. Surf. Sci. 225:176–185. https://doi.org/ 10.1016/j.apsusc.2003.10.007.

Aslam R. , M. Mobin , Huda, et al. 2020. Ionic liquids derived from α-amino acid ester salts as potent green CIs for mild steel in 1M HCl. J. Mol. Liq.318:113982. https://doi.org/10.1016/j.molliq.2020.113982.

Ateya, B.G., El-Anadouli, B.E., El-Nizamy, F.M., 1984. The adsorption of thiourea on mild steel. Corros. Sci. 24, 509. https://doi.org/10.1016/0010-938X(84)90033-7.

Becke, A.D., 1993. Density-functional thermochemistry. III. The role of exact exchange. J. Chem. Phys. 98, 5648–5652. https://doi.org/10.1063/1.464913.

Cao, C., 1996. On electrochemical techniques for interface inhibitor reserch. Corros. Sci. 38 (12), 2073–2082. https://doi.org/10.1016/S0010-938X(96)00034-0.

Cao, Y., Zou, C., Wang, C., et al, 2021. Green CI of β-cyclodextrin modified xanthan gum for X80 steel in 1 M H_2SO_4 at different temperature. J. Mol. Liq. 341,. https://doi.org/10.1016/j.-molliq.2021.117391 117391.

Chaudhary, S., Tak, R.K., 2021. Natural corrosion inhibition and adsorption characteristics of tribulus terrestris plant extract on aluminium in hydrochloric acid environment. Biointerface Res. Appl. Chem. 12, 2603–2617. https://doi.org/10.33263/BRIAC122.26032617.

Chen, S., Zhao, H.J., Chen, S.Y., et al, 2020. Camphor leaves extract as a neoteric and environment friendly inhibitor for Q235 steel in HCl medium: Combining experimental and theoretical researches. J. Mol. Liq. 312,. https://doi.org/10.1016/j.molliq.2020.113433 113433.

Dehghani, A., Bahlakeh, G., Ramezanzadeh, B., 2019. A detailed electrochemical/ theoretical exploration of the aqueous Chinese gooseberry fruit shell extract as a green and cheap CI for mild steel in acidic solution. J. Mol. Liq. 282, 366–384. https://doi.org/10.1016/j.molliq.2019.03.011.

Dong, S., Yang, Y., Liang, T., et al, 2021. Construction and corrosion resistance of Ni-B4C superhydrophobic composite coatings on Q235 steel. Surf. Coating. Technol. 422 (127551). https://doi.org/10.1016/j.surfcoat.2021.127551.

Eddy N.O., Awe F.E., Gimba C.E., et al. 2011. QSAR, Experimental and computational chemistry simulation studies on the inhibition potentials of some amino acids for the corrosion of mild steel in 0.1 M HCl, Int. J. Electrochem. Sci. 6:931–957. Corpus ID: 222281566.

El-Asri, A., Rguiti, M.M., Jmiai, A., et al, 2023. Carissa macrocarpa extract (ECM) as a new efficient and ecologically friendly CI for copper in nitric acid: Experimental and theoretical approach. J. Taiwan Inst. Chem. Eng. 142, 104633.

Elgyar, O.A., Ouf, A.M., El-Hossiany, A., et al, 2021. The inhibition action of viscum album extract on theCorrosion of carbon steel in hydrochloric acid solution. Biointerface Res. Appl. Chem. 11, 14344–14358. https://doi.org/10.33263/BRIAC116.1434414358.

Fadhil, A.A., Khadom, A.A., Liu, H., et al, 2019. (S)-6-Phenyl-2,3,5,6-tetrahydroimidazo[2,1-b] thiazole hydrochloride as CI of steel in acidic solution: gravimetrical, electrochemical, surface morphology

and theoretical simulation. J. Mol. Liq. 276, 503–518. https://doi.org/10.1016/j.molliq.2018.12.015.

Fatma, K., Ramazan, S., İbrahim, H.G., 2023. The use of methanol extract of Rheum Ribes (Işgın) flower as a natural and promising CI for mild steel protection in 1 M HCl solution. J. Ind. Eng. Chem. 122, 102–117. https://doi.org/10.1016/J.JIEC.2023.02.013.

Frontini, M.A., Schreiner, W., Vázquez, M., et al, 2019. Nitrite corrosion inhibition in chloride-rich electrolytes correlated to the electrical properties of surface films on carbon steel. Construct. Build. Mater. 227,. https://doi.org/10.1016/j.conbuildmat.2019.08.031 116650.

Ghahremani, P., Tehrani, M.E.H.N., Ramezanzadeh, M., et al, 2021. Golpar leaves extract application for construction of an effective anti-corrosion film for superior mild-steel acidic-induced corrosion mitigation at different temperatures. Colloids Surf. A Physicochem. Eng. Asp. 629,. https://doi.org/10.1016/j.colsurfa.2021.127488 127488.

Grimme S., Ehrlich S., Goerigk L., 2011. Effect of the damping function in dispersion corrected density functional theory, J. Comp. Chem. 32:1456-1465. https://doi: 10.1002/jcc.21759.

Hamilton-Aamachree, A., Iroha, N.B., 2020. Corrosion inhibition of API 5L X80 pipeline steel in acidic environment using aqueous extract of Thevetia peruviana. Chem. Int. 6 (3), 117–128. https://doi.org/10.5281/zenodo.3516565.

Hang, X., Li, W., Yu, G., et al, 2020. Evaluation of Idesia polycarpa Maxim fruits extract as a natural green CI for copper in 0.5 M sulfuric acid solution. J. Mol. Liq. 318 (114080). https://doi.org/10.1016/j.molliq.2020.114080.

Haque, J., Verma, C., Srivastava, V., 2021. Corrosion inhibition of mild steel in 1M HCl using environmentally benign Thevetia peruviana flower extracts. Sustain. Chem. Pharm. 19,. https://doi.org/10.1016/j.scp.2020.100354 100354.

Hossain N., Chowdhury M.A., Kchaou M., 2020.An overview of green CIs for sustainable and environment friendly industrial development. J. Adhes. Sci. Technol. 35:673–690. https://doi.org/10.1080/01694243.2020.1816793.

Hu, K., Zhuang, J., Ding, J., 2017. Influence of biomacromolecule DNA CI on carbon steel. Corros. Sci. 125, 68–76. https://doi.org/10.1016/j.corsci.2017.06.004.

Indra, P.P., Vinod Kumar, K.P., Sudha, K.S., 2019. Studies of the anticorrosive nature of green Ricinus seed extract with neem biodiesel in copper metal. Biofuels 12, 559–568. https://doi.org/10.1080/17597269.2018.1506634.

Ituen, E.B., Solomon, M.M., Umoren, S.A., et al, 2019. Corrosion inhibition by amitriptyline and amitriptyline based formulations for steels in simulated pickling and acidizing media. J. Pet. Sci. Eng. 174, 984–996. https://doi.org/10.1016/j.petrol.2018.12.011.

Khaled, K.F., Abdelshafi, N.S., El-Maghraby, A.A., et al, 2012. Alanine as CI for iron in acid medium: a molecular level study. Int. J. Electrochem. Sci. 7, 12706–12719 www.electrochemsci.org.

Kharitonov, D.S., Dobryden, I., Sefer, B., et al, 2020. Surface and corrosion properties of AA6063-T5 aluminum alloy in molybdate-containing sodium chloride solutions. Corrosion Sci. 171,. https://doi.org/10.1016/j.corsci.2020.108658 108658.

Koudelka, M., Sanchez, J., Augustyński, J., 2019. On the nature of surface films formed on iron in aggressive and inhibiting polyphosphate solutions. J. Electrochem. Soc. 129 (6), 1186–1191.

Li B,Y., Wang W., Chen L.P. et al. 2023. Corrosion inhibition effect of magnolia grandiflora leaves extract on mild steel in acid solution. Int. J. Electrochem. Sci.,18(4): 100082.https://doi.org/ 10.1016/J.IJOES.2023.100082.

Lin B,L. , Shao J.J. , Zhao C. et al. 2023. Passiflora edulis Sims peel extract as a renewable CI for mild steel in phosphoric acid solution. J. Mol. Liq. 375 : 121296. https://doi.org/ 10.1016/j.molliq.2023.121296

Liu, Z., Ye, Y.W., Chen, H., 2020. Corrosion inhibition behavior and mechanism of N-doped carbon dots for metal in acid environment. J. Clean. Prod. 270,. https://doi.org/10.1016/j.jclepro.2020.122458 122458.

Liu, X., Zheng, J., Fu, J., et al, 2018. Multi-level optimization of maintenance plan for natural gas pipeline systems subject to external corrosion. J. Nat. Gas Sci. Eng. 50, 64–73. https://doi.org/10.1016/j.jhazmat.2018.09.044.

Majd, M.T., Ramezanzadeh, M., Ramezanzadeh, B., et al, 2020. Production of an environmentally stable anti-corrosion film based on Esfand seed extract molecules-metal cations: integrated experimental and computer modeling approaches. J. Hazard Mater. 382,. https://doi.org/10.1016/j.jhazmat.2019.121029 121029.

Mobin, M., Ahmad, I., Basik, M., et al, 2020. Experimental and theoretical assessment of almond gum as an economically and environmentally viable CI for mild steel in 1 M HCl. Sustain. Chem. Pharm. 18,. https://doi.org/10.1016/j.scp.2020.100337 100337.

Mohammad, A.B., Mahboobeh, A., Maryam, R., 2021. An enhancement on corrosion resistance of low carbon steel by a novel bio-inhibitor (leech extract) in the H_2SO_4 solution. Surfaces and Interface 24,. https://doi.org/10.1016/j.surfin.2021.101159 101159.

Mourya, P., Banerjee, S., Singh, M.M., 2014. Corrosion inhibition of mild steel in acidic solution by Tagetes erecta (Marigold flower) extract as a green inhibitor. Corros. Sci. 85, 352–363. https://doi.org/10.1016/j.corsci.2014.04.036.

Nasser H., Van Steen C., Vandewalle , E. 2021.Verstrynge. An experimental assessment of corrosion damage and bending capacity reduction of singly reinforced concrete beams subjected to accelerated corrosion. Construct. Build. Mater. 286:122773. https://doi.org/10.1016/ j.conbuildmat. 2021.122773.

Neese, F., 2018. Software update: the ORCA program system, version 4.0. WIREs Comput. Mol. Sci. 8, 1327. https://doi.org/10.1002/wcms.1327.

Obi-Egbedi, N.O., Obot, I.B., 2011. Inhibitive properties, thermodynamic and quantum chemical studies of alloxazine on mild steel corrosion in H_2SO_4. Corros. Sci. 53, 263–275. https://doi.org/10.1016/j.corsci.2010.09.020.

Olasunkanmi, L.O., Ebenso, E.E., 2020. Experimental and computational studies onpropanone derivatives of quinoxalin-6-yl-4,5-dihydropyrazole as inhibitors of mild steel corrosion in hydrochloric acid. J. Colloid Interface Sci. 561, 104–116. https://doi.org/10.1016/j.jcis.2019.11.097.

Qiang, Y., Li, H., Lan, X., 2020. Self-assembling anchored film basing on two tetrazole derivatives for application to protect copper in sulfuric acid environment. J. Mater. Sci. Technol. 52, 63–71. https://doi.org/10.1016/j.jmst.2020.04.005.

Saleh, M.M., Mahmoud, M.G., Abd El-Lateef, H.M., 2019. Comparative study of synergistic inhibition of mild steel and pure iron by 1-hexadecylpyridinium chloride and bromide ions. Corrosion Sci. 154, 70–79. https://doi.org/10.1016/j.corsci.2019.03.048.

Salleh S.Z., Yusoff A.H., Zakaria S.K.,2021. Plant extracts as green CI for ferrous metal alloys: a review. J. Clean. Prod. 304:127030. https://doi.org/10.1016 j.jclepro.2021.127030.

Sanaei, Z., Ramezanzadeh, M., Bahlakeh, G., et al, 2019. Use of Rosa canina fruit extract as a green CI for mild steel in 1 M HCl solution: a complementary experimental, molecular dynamics and quantum mechanics investigation. J. Ind. Eng. Chem. 69, 18–31. https://doi.org/10.1016/j.jiec.2018.09.013.

Schaefer A., Huber C., Ahlrichs R.,1994. Fully optimized contracted Gaussian-basis sets of triple zeta valence quality for atoms Li to Kr, J. Chem. Phys. 100:5829-5835. https://doi.org/ 10.1063/ 1.467146.

Schaefer, A., Horn, H., Ahlrichs, R., 1992. Fully optimized contracted Gaussian-basis sets for atoms Li to Kr. J. Chem. Phys. 97, 2571–2577. https://doi.org/10.1063/1.463096.

Silva, M.V.L.D., Policarpi, E.D.B., Spinelli, A., 2021. Syzygium cumini leaf extract as an eco-friendly CI for carbon steel in acidic medium. J. Taiwan Inst. Chem. Eng. 129, 342–349. https://doi.org/10.1016/j.jtice.2021.09.026.

Somers, A.E., Hinton, B.R.W., Bruin-Dickason, C., et al, 2018. New, environmentally friendly, rare earth carboxylate CIs for mild steel. Corrosion Sci. 139, 430–437. https://doi.org/10.1016/j.corsci.2018.05.017.

Sun C.Y., 2011. Preparation and Study on infrared spectra of Zinc pheophorbin. J.Tangshan Tea Colle., 33:34-36. 1009-9115(2011)05-0034-03.

Tan, B.C., Xiang, B., Zhang, S.T., et al, 2021 (a). Papaya leaves extract as a novel eco-friendly CI for Cu in H_2SO_4 medium. J. Colloid Interface Sci. 582, 918–931. https://doi.org/10.1016/j.jcis.2020.08.093.

Tan, B.C., He, J.H., Zhang, S.T., et al, 2021 (b). Insight into anti-corrosion nature of Betel leaves water extracts as the novel and eco-friendly inhibitors. J. Colloid Interface. Sci. 585, 287–301. https://doi.org/10.1016/j.jcis.2020.11.059.

Umoren, S.A., Obot, I.B., Madhankumar, A., et al, 2015. Performance evaluation of pectin as ecofriendly CI for X60 pipeline steel in acid medium: Experimental and theoretical approaches. Carbohyd. Polym. 124, 280–291. https://doi.org/10.1016/j.carbpol.2015.02.036.

Wang, Q., Tan, B., Bao, H., et al, 2019. Evaluation of Ficus tikoua leaves extract as an eco-friendly CI for carbon steel in HCl media. Bioelectrochemistry 128, 49–55. https://doi.org/10.1016/j.bioelechem.2019.03.001.

Wu P., Han J. Y., Chen H.X., 2016. Extraction of chlorophyll from spinach and its ultraviolet spectrum. Guangzhou Chem. Ind., 44:144-145. 1001-9677(2016)019-0144-02.

Xomet, O.O., Aguilar, C.L., González, P.H., et al, 2014. Adsorption and corrosion inhibition performance by three new ionic liquids on api 5l X52 steel surface in acid media. Ind. Eng. Chem. Res. 53, 9534–9543. https://doi.org/10.1021/ie4035847.

Xu, X., Liu, S.M., Smith, K., et al, 2020. An overview on corrosion of iron and steel components in reclaimed water supply systems and the mechanisms involved. J. Clean. Prod. 276,. https://doi.org/10.1016/j.jclepro.2020.124079 124079.

Yadav, D.K., Maiti, B., Quraishi, M.A., 2010. Electrochemical and quantum chemical studies of 3,4-dihydropyrimidin-2(1H)-ones as CIs for mild steel in hydrochloric acid solution. Corros. Sci. 52, 3586–3598. https://doi.org/10.1016/j.corsci.2010.06.030.

Ye, Y., Zhang, D., Zou, Y., et al, 2020. feasible method to improve the protection ability of metal by functionalized carbon dots as environmentfriendly CI. J. Clean. Prod. 264,. https://doi.org/10.1016/j.jclepro.2020.121682 121682.

Yilmaz N., Fitoz A., ErgunÜ., et al. 2016. A combined electrochemical and theoretical study into the effect of 2-((thiazole-2-ylimino) methyl)phenol as a CI for mild steel in a highly acidic environment, Corros. Sci. 111:110-120. https://doi.org/10.1016/j.corsci.2016.05.002.

Zhang K., Yang W., Yin X., 2018. Amino acids modified konjac glucomannan as green CIs for mild steel in HCl solution, Carbohyd. Polym. 181:191-199. https://doi. org/10.1016/j.carbpol.2017.10.069.

Zhang F., Xu X., Lei R., et al, 2022. Inhibition Effect of Orange Peel Extract on Aluminum in Hydrochloric Acid Solution. J. Southwest Forestry University,42:1-8. https://doi.10.11929/ j.swfu.202101009

Zhang, Q.H., Hou, B.S., Zhang, G.A., 2020. Inhibitive and adsorption behavior of thiadiazole derivatives on carbon steel corrosion in CO_2 -saturated oilfield produced water: effect of substituent group on efficiency. J. Colloid Interface Sci. 572, 91–106. https://doi.org/10.1016/j.jcis.2020.03.065.

Zhang, S.H., Liu, S.J., Zhu, Z.X., et al, 2017. Research on the extraction condition and corrosion inhibition performance of actire principle in pomelo peel. Fine Speci. Chem. 25, 27–32. https://doi.org/10.19482/j.cn11-3237.2017.01.05.